The coordination of Mg in foraminiferal calcite

Oscar Branson [a,*], Simon A.T. Redfern [a], Tolek Tyliszczak [b], Aleksey Sadekov [a], Gerald Langer [a], Katsunori Kimoto [c], Henry Elderfield [a]

[a] Department of Earth Sciences, University of Cambridge, Downing St, Cambridge CB2 3EQ, UK
[b] Advanced Light Source, Lawrence Berkeley National Laboratory, Berkeley, CA 94720, USA
[c] Research Institute for Global Change, JAMSTEC, 2-15 Natsushima-cho, Yokosuka, 237-0061, Japan

ABSTRACT

The Mg/Ca ratio of foraminiferal calcite is a widely accepted and applied empirical proxy for ocean temperature. The analysis of foraminifera preserved in ocean sediments has been instrumental in developing our understanding of global climate, but the mechanisms behind the proxy are largely unknown. Analogies have been drawn to the inorganic precipitation of calcite, where the endothermic substitution of Mg for Ca is favoured at higher temperatures. However, evidence suggests that foraminiferal Mg incorporation may be more complex: foraminiferal magnesium is highly heterogeneous at the sub-micron scale, and high Mg areas coincide with elevated concentrations of organic molecules, Na, S and other trace elements. Fundamentally, the incorporation mode of Mg in foraminifera is unknown. Here we show that Mg is uniformly substituted for Ca within the calcite mineral lattice. The consistency of Mg-specific X-ray spectra gathered from nano-scale regions across the shell ('test') reveals that the coordination of Mg is uniform. The similarity of these spectra to that produced by dolomite shows that Mg is present in an octahedral coordination, ideally substituted for Ca in a calcite crystal structure. This demonstrates that Mg is heterogeneous in concentration, but not in structure. The degree of this uniformity implies the action of a continuous Mg incorporation mechanism, and therefore calcification mechanism, across these compositional bands in foraminifera. This constitutes a fundamental step towards a mechanistic understanding of foraminiferal calcification processes and the incorporation of calcite-bound palaeoenvironment proxies, such as Mg.

© 2013 The Authors. Published by Elsevier B.V. Open access under CC BY license.

1. Introduction

The Mg/Ca ratio of foraminiferal calcite is a widely accepted and applied empirical proxy for ocean temperature (Bohaty et al., 2012; Elderfield and Ganssen, 2000; Garidel-thoron et al., 2005; Lea et al., 2000; Nürnberg et al., 2000). The construction of Mg/Ca records from foraminifera preserved in ocean sediments has been instrumental in developing our understanding of global climate, but the mechanisms behind the proxy have remained largely unknown. Use and interpretation of the Mg/Ca palaeothermometer is based on the assumption that Mg is inorganically hosted in the calcite mineral lattice, but foraminiferal Mg/Ca ratios differ significantly from those derived from inorganic precipitation experiments (Bohaty et al., 2012; Elderfield and Ganssen, 2000; Garidel-thoron et al., 2005; Lea et al., 1999, 2000; Morse and Bender, 1990; Nürnberg et al., 2000). Most foraminifera contain orders of mag-

nitude less Mg (Morse and Bender, 1990), Mg in foraminiferal calcite is around three times more sensitive (up to ∼10% per °C) to temperature change (Lea et al., 1999), and both Mg concentration and temperature sensitivity show high inter- (Morse and Bender, 1990) and intra-species (Elderfield et al., 2002) variability between organisms inhabiting similar environments (Hintz et al., 2006; Kısakürek et al., 2008; Lea et al., 1999; Russell et al., 2004). These disparities are labelled 'vital effects' (Urey et al., 1951; Weiner and Dove, 2003), and are broadly attributed to biological mechanisms that influence the calcification process. As long as the offsets caused by 'vital effects' are systematic, and remain consistent within species, they can be overcome by robust calibration studies (Anand et al., 2003; Elderfield et al., 2006; Nürnberg et al., 1996), and do not represent an insurmountable barrier to the application of the palaeothermometer. However, evidence suggests that foraminiferal Mg incorporation may be more complex: foraminiferal Mg is highly heterogeneous at the sub-micron scale (Eggins et al., 2004; Erez, 2003; Kunioka et al., 2006; Sadekov et al., 2005), and high Mg areas coincide with elevated concentrations of organic molecules, Na, S and other trace elements (Erez, 2003; Kunioka et al., 2006). Internal heterogeneity is both diverse, with different species exhibiting either systematic
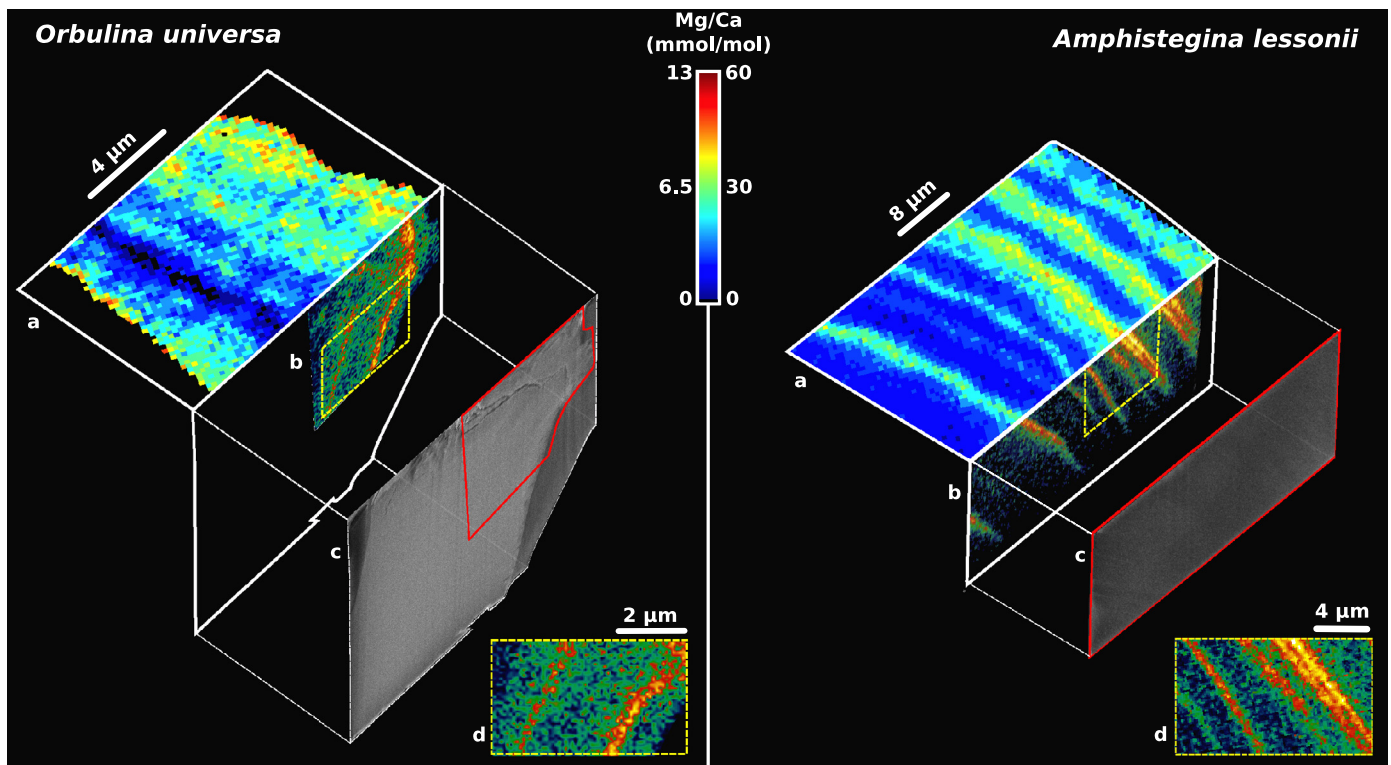
Fig. 1. The distribution of Mg in foraminifera. Electron microprobe maps of the samples reveal patterns of Mg/Ca banding (A), which are in agreement with Scanning Transmission X-ray Microscope (STXM) images of Mg-Specific X-ray absorption (B, arbitrary units) in the thin-section samples (C). This confirms that the STXM Mg signal is real, and not an artefact of sample density or thickness variations. This is evident in the uniformity of the off-peak STXM Optical Density (OD) images of the thin section samples (C). In (C) brightness is a function of absorbed photons, and the dark areas either side of the *Orbulina* specimen are sections of the resin used to mount the samples. Magnified areas of the STXM images denoted by dashed yellow boxes show the length scale of Mg heterogeneity to be in the order of 1–300 nm (D). The Mg bands in the *Amphistegina* specimen (B and D) taper towards the bottom of the image. This reflects a decrease in sample thickness, not a reduction in Mg content. The *Amphistegina* (B) image was taking in transmission mode (25 nm Zone Plate, 150 nm step, 2 ms dwell), and the *Orbulina* (B) image in fluorescence mode (40 nm Zone Plate, 100 nm step, 50 ms dwell). The colour scale bar denotes Mg/Ca in the electron microprobe maps (A), and the STXM images are in arbitrary units.

banding (Fig. 1) or apparently random variations (Sadekov et al., 2005), and large, with [Mg] varying by up to a factor of 10 across the test. The coincidence of Mg enrichment with high concentrations of other trace elements and organic molecules (Erez, 2003; Kunioka et al., 2006) raises the possibility that Mg is incorporated in association with these other components, rather than directly substituted for Ca. If Mg exists in association with organics, Na or S, or in a coordination other than ideally substituted into calcite, the connections drawn between modern and fossil species by the application of empirical calibrations must be questioned. Furthermore, if the coordination of Mg differs between the high-Mg ('on-band') and low-Mg ('off-band') regions, this would imply a complex two-phase incorporation mechanism, which would invalidate the inorganic precipitation analogies. The small size (typically <500 μm Ø, walls 5–50 μm thick) and high purity (>99% CaCO$_3$) of foraminifera has thus far precluded the direct mineralogical investigation of foraminiferal Mg. Here we apply nanoscale synchrotron X-ray spectroscopy techniques to address the fundamental uncertainties raised by internal Mg/Ca heterogeneity, by conducting a nano-scale mineralogical investigation of the atomic coordination of Mg in on- and off-band regions through the foraminiferal test.

2. Methodology

We characterise the coordination of Mg in two disparate species of symbiont-bearing foraminifera using Near-Edge X-ray Absorption Fine Structure (NEXAFS) spectroscopy. Both the benthic *Amphistegina lessonii* (∼40 mmol/mol Mg/Ca) and the planktic *Orbulina universa* (1–10 mmol/mol Mg/Ca) are known to exhibit sys-

tematic Mg banding (Eggins et al., 2004; Erez, 2003; Kunioka et al., 2006; Sadekov et al., 2005), which was confirmed in our specimens by electron microprobe maps (Fig. 1A). Test cross-sections were prepared using a focused ion beam (FIB, Fig. 1C), and analysed using a scanning transmission X-ray microscope (STXM, Fig. 1B and D).

2.1. Sample preparation

Recently alive specimens of *Orbulina universa* and *Amphistegina lessonii*. were obtained from plankton tow samples and cultures, respectively. Individual tests were broken into several pieces with a fine scalpel blade in ethanol, and the fragments mounted on double-sided tape with the flattest broken edge in plane with the tape surface (so the majority of the fragment protruded normal to the tape surface). These mounted fragments were set in epoxy resin following a standard procedure for preparing petrographic samples. The set resin blocks were cleaned with petroleum ether to remove traces of the tape adhesive, and polished to expose the edges of the test fragments. The polished surface was carbon coated, and imaged in an SEM to guide the location of the sample fragments in a focused ion beam (FIB) instrument.

Sections were cut bisecting the test wall perpendicular to the polished surface in a Helios NanoLab FIB, following a modification of FEI™'s standard procedure for producing and extracting TEM samples (Reyntjens, 2006). Deviations from the normal methods were necessary because the foraminifera sections were wedge shaped, and larger and thicker than normal TEM sections. Wedge-shaped samples were required to allow for uncertainties in the required sample thickness for STXM analysis.

A protective platinum layer was deposited on the polished surface and rough trenches were cut on three sides of the sample using the highest available current (30 kV, 21 nA). The section shape refined using a 9.3 nA beam, leaving a 4 μm thick section which was cut out with a 2.8 nA beam and transferred to a TEM grid using an Omniprobe™ micromanipulator. Once attached to the TEM grid with platinum, a series of angled polishing cuts were made to form the sample into the desired wedge shape. These cuts were made at 0.92 and 0.46 nA (both at 30 kV), decreasing the current as the sample neared completion. The final sections thinned from approximately 2 μm to extinction along their shortest axis.

The FIB milling process is known to leave an amorphous damaged layer on the surface of the specimen (McCaffrey et al., 2001). The thickness of the damaged layer is proportional to the beam energy, and varies with the angle of the beam relative to the sample (McCaffrey et al., 2001). A 30 kV beam was used at all sample preparation stages for speed, and low angle milling (beam parallel to sample) was employed to minimise the angle component of sample damage. This milling setup is estimated to leave 20–24 nm of amorphous damaged material on the sample surface (Gao et al., 2004; Giannuzzi et al., 2005). All X-ray analyses were performed on sections of the sample >1.8 μm thick, so this damaged layer comprised <3% of the analysed material. Previous studies have obtained meaningful STXM and TEM data from FIB-prepared biogenic calcite samples (Benzerara et al., 2011; Kudo et al., 2010; Obst et al., 2009), suggesting this damage layer should not significantly influence our results.

2.2. Electron probe mapping

Electron probe maps were taken from the polished resin blocks adjacent to the site of FIB milling. The scan setup was modified from a previous study (Sadekov et al., 2005), employing a finer beam (∼1 μm Ø), and a smaller step size (0.5 μm).

2.3. STXM data acquisition and analysis

Data were gathered at the STXM branch of beamline 11.0.2 at the Advanced Light Source (ALS, Berkeley, CA) (Bluhm et al., 2006). This instrument has a spatial resolution of 30 nm, which allowed us to map the Mg bands in fine detail (Fig. 1B and D), and extract NEXAFS spectra from precise on- and off-band regions to examine Mg coordination. A NEXAFS spectrum measures the absorption of X-rays at and above (to +150 eV) the ionization energy (or 'absorption edge') of an element. Specific elements within a sample can be targeted because of their unique ionization energies. The position of the absorption edge is influenced by the electronic structure of the atom, and features of the post absorption edge region are defined by multiple scattering from the atom's next-nearest-neighbours. The features of a NEXAFS Mg-spectrum are determined by the Mg coordination: the number, arrangement and species of its nearest-neighbour atoms, and in turn their environment (what else they are bonded to) – everything that influences the local electronic structure around the atom of interest. In the consideration of these Mg spectra, it is important to note that only the immediate environment around the Mg is relevant, and not the long-range structure of the whole phase.

All samples were mounted on aluminium STXM sample holders. The TEM mounts containing the foraminiferal sections were attached using carbon tape, and powder reference samples were applied to Silson™ 100 nm Si_3N_4 TEM windows fastened to the sample mounts with rapid setting epoxy. Prior to data acquisition the sample chamber was evacuated (to 40 Pa) and flooded with He gas to 34–50 kPa to minimise X-ray absorption in air. STXM images and NEXAFS spectra were collected in both transmission (Bluhm et al., 2006) and fluorescence (Hitchcock et al., 2010) modes. Transmitted X-rays were collected using a scintillation counter, operating in pulse counting mode at low flux (<20 MHz), and in analogue mode at higher fluxes while in fluorescence mode (>20 MHz). In fluorescence mode emitted X-rays were collected using a front-mounted Amptek™ X123 Super-SDD detector, recording Mg Kα (1254 eV) and Kβ (1302 eV) emission bands. Zone Plates were 25 and 40 nm in transmission and fluorescence modes, respectively. The 25 nm Zone Plate gave the best spatial resolution (∼30 nm spot size), but the short working distance (1000–1200 μm) and lower flux made it unsuitable for use with the fluorescence detector. The 40 nm Zone Plate decreased the spatial resolution (to ∼45 nm), but lengthened the working distance (2000 μm) to physically accommodate the front-mounted Amptek™ detector and minimise the background scatter it picked up from the OSA, and allowed a higher flux, which improved fluorescence data quality.

STXM images presented here (Fig. 1) were taken after a rough NEXAFS spectrum was recorded to find the position of the Mg K-edge. They are presented as simple absorption maps, as the wedge shape of the samples precludes the meaningful interpretation of optical density maps of the whole section.

Samples were analysed following a standard procedure: a series of STXM images were taken at the Mg K-edge (∼1314 eV) with increasing spatial resolution to locate a region of interest (in transmission mode, an area with 30–90% absorption). NEXAFS spectra were then collected by taking either a stack of images or line transects at a series of energy steps across the absorption edge. In absorption mode the acquisition area always included an off-sample region for background (I_0) normalisation, and conversion to optical density ($OD = -\log(I/I_0)$). This was not necessary in fluorescence mode, as the variations in fluorescence I_0 over the energy range considered are negligible. Absorption spectra were normalised to I_0 and extracted from the image stacks or line scans using the aXis2000 IDL™ widget package (Hitchcock, 1997). For the reference materials, if the quality of a single spectrum was poor extra spectra were collected, and data summed to improve quality, effectively increasing the pixel count time. All spectra collected during the experiment can be seen in Fig. 2.

Spectrum processing, fitting, analysis and graphing were performed in R (R Core Team, 2012; RStudio, 2013). The presented on- and off-band Mg spectra are averages of multiple on- and off-band regions to improve data quality. On- and off-band regions were selected by hand, leaving an unselected margin on the edges of the bands (Fig. S1). To ensure the size or shape of the selection area did not influence the resulting spectra, multiple sizes and shapes of selection were compared, and in all cases the results were the same. Prior to analysis all spectra were normalised so their range was 0 to 1. Before normalisation, the maximum optical density in any spectra was 1.75, well below the level where saturation effects are seen on this beamline (above 2.4–2.6). Specimen spectra were fitted with combinations of reference spectra and a linear background using a linear least squares model (lm). Data were collected over a period of reduced beam stability, which introduced a variable error in energy accuracy between the samples, particularly between samples collected in different beamtime shifts. To account for this uncertainty, all but one spectrum (dolomite) were allowed to drift by up to ±0.5 eV during the fitting process. A detailed assessment of our fitting algorithm can be found in the supplementary material. The dolomite spectrum was the major component of all fits, and was used as an internal energy standard.

There is some uncertainty surrounding the relative scaling of peak intensities with Mg concentration in different Mg-bearing phases, and therefore the sensitivity of the technique to detecting combinations of different Mg coordination states. Most candidate phases had peaks that were distinct from the sample spectra, and their presence would have been clearly manifest in a systematic
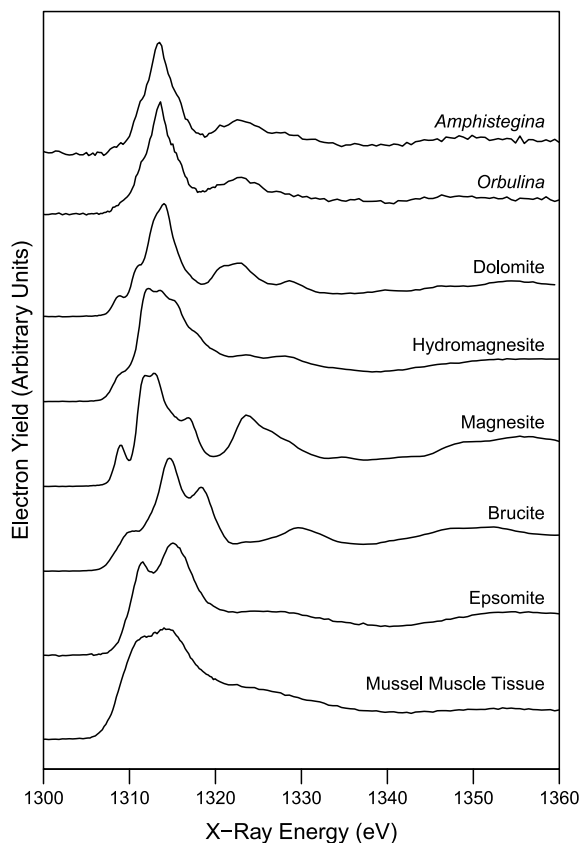
Fig. 2. Mg NEXAFS spectra. The normalised Mg K-edge NEXAFS spectra collected from the samples and reference materials in this study. The sample spectra are at the top, and the reference spectra presented in descending order based on their similarity to the sample spectra.
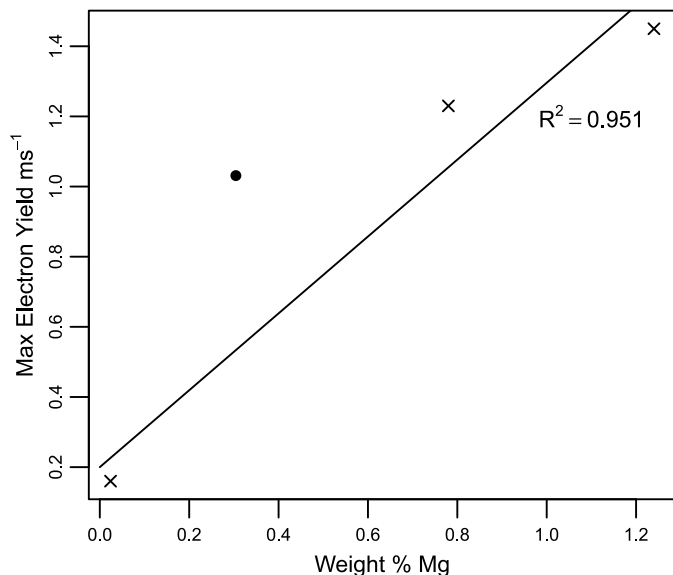

Fig. 3. The detection of organic-hosted Mg. The count-normalised 1314 eV Mg peak height from 3 biogenic calcites (foraminifera and two echinoderm samples) is shown as a function of weight% Mg. Peak height shows a linear increase with Mg concentration, which is unsurprising as the linearity of this relationship underlies electron-probe and XRF techniques. The count-normalised Mg peak height from our organic reference material (muscle tissue of *Mytilus edulis*) produced a disproportionately intense peak, implying that our method was *more* sensitive to organic-hosted Mg than calcite-hosted Mg, and rendering the detection of organic-hosted Mg in our spectra feasible.
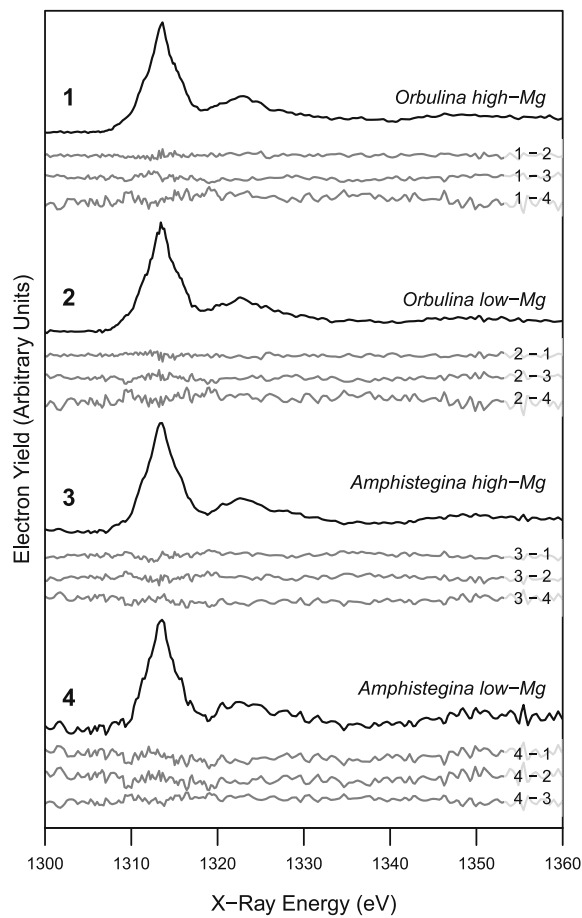

Fig. 4. Uniform Mg coordination. Normalized Mg K-edge NEXAFS spectra collected from high- and low-Mg bands in *O. universa* (1 and 2) and *A. lessonii* (3 and 4) reveal that Mg is coordination is uniform throughout the test. The residuals comparing each scan to all others are shown, with their identity denoted by the numbers on the right hand side. The spectra are identical to within instrumental error, as is evident in the featureless (within the instrumental noise) residuals.

modification of the Mg peak shape. However, organic matter produces a diffuse, featureless peak (Fig. 2), as it does not contain Mg in a well-defined coordination. This would be hard to detect if the organic spectra were also very weak. To explore this, we examined the relationship between Mg peak intensity and Mg concentration in biogenic Mg-calcite and organic matter (Fig. 3). This reveals that the technique is more sensitive to organic-hosted Mg than calcite-hosted Mg, demonstrating that organic-hosted Mg would be apparent if it were significantly present in the high-Mg bands. Fluorescence spectra will exhibit a similar trend, as they are governed by the same physical principles.

3. Results

Raster X-ray absorption images map Mg distribution at much higher resolution than the electron microprobe (Fig. 1B and D vs. A). This high-resolution mapping reveals that the broad (∼2–3 μm) Mg rich bands observed in *A. lessonii* by the electron probe were in fact made up of sequential finer (<500 nm) bands in close proximity, revealing that banding is much finer-grained than previously thought (Sadekov et al., 2005).

Spectra gathered from on- and off-band regions in *A. lessonii* and *O. universa* were identical within instrumental error, as is evident from the featureless (to within instrumental noise) residuals in Fig. 4.

A linear-least-squares fitting procedure was used to compare the spectra of foraminiferal Mg to those of reference materials with
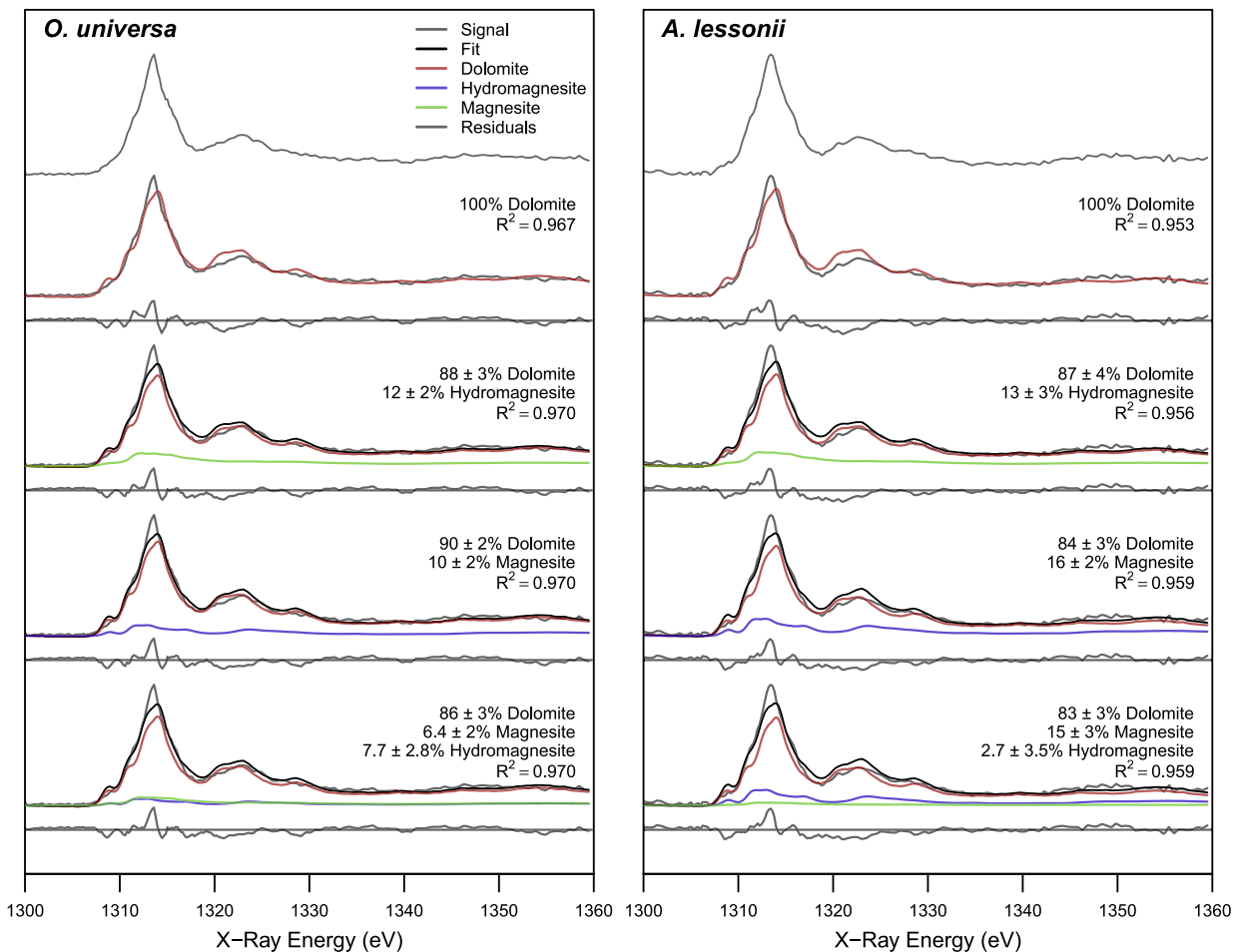
Fig. 5. Identifying the Mg environment. We compare of the local Mg environment in *O. universa* and *A. lessonii* to the candidate minerals dolomite, hydromagnesite and magnesite. The normalized Mg K-edge NEXAFS spectrum from foraminiferal Mg is shown at the top, with mixtures of candidate mineral spectra determined by linear least squares fitting displayed below. Each fit consists of one or more candidate spectra combined with a linear background. The dolomite spectrum alone is a good fit for the foraminiferal Mg, although not perfect. The fit is marginally improved by including extra materials in the mixture, but importantly the shape of the residuals (shown below each model on the same scale) does not alter significantly, and the increase in goodness of fit (indicated by R^2) is minimal.

known Mg coordination (Figs. 2 and 5). Both individual reference spectra, and mixtures of reference spectra were considered in the fitting model. The foraminiferal Mg spectrum was most similar to that of dolomite (Fig. 5), although the fit was not perfect in either *O. universa* or *A. lessonii* ($R^2 = 0.967$ and 0.953, respectively). The fit was either marginally improved (in *A. lessonii*) or not affected (in *O. universa*) by the inclusion of minor hydromagnesite and magnesite components in the model (indicated by R^2 values in Fig. 5). The inclusion of spectra from brucite, epsomite and *Mytilus edulis* tissue were detrimental to the fit.

4. Discussion

First, we address the question of whether the observed differences in Mg concentration (Fig. 1) are accompanied by variations in Mg coordination, by comparing NEXAFS spectra gathered from on- and off-band regions. The Mg banding could either be produced by variations in the concentration of Mg hosted in a single phase, or be the result of a multi-host-phase system, where a background Mg environment is augmented by an alternate Mg host phase in the bands. Our reference NEXAFS spectra demonstrate the sensitivity of this technique to changes in the coordination and speciation of atoms around Mg: closely related mineral phases produce disparate spectra (Fig. 2). Therefore, we would expect a single-host-phase system (Mg in a single coordination) to produce uniform spectra throughout the test, and the spectra produced by a

multi-host-phase system (with multiple Mg coordinations) to vary between the on- and off-band regions. The coincidence of Mg, S, Na and organic maxima in the test (Erez, 2003) suggests that Mg is structurally associated with these other components in the high-Mg bands, and thus exists in a two-phase system. Our data, however, conclusively demonstrate that the coordination of Mg is uniform across the banding of individual tests and between the two species (Fig. 4). This reveals that intra-test Mg heterogeneity does not result from a multi-host Mg incorporation system, but is driven by variations in the concentration of Mg in a single coordination. The similarity between these two disparate species also suggests that these results are more broadly applicable to other foraminifera that exhibit Mg banding (Sadekov et al., 2005).

The uniformity of Mg coordination reveals that Mg is hosted in a single atomic environment in foraminifera, but the nature of this environment is unknown. To address this second problem, we compare the foraminiferal Mg spectra to those of various model materials: dolomite, magnesite, hydromagnesite, brucite, epsomite and organic material (the muscle tissue of *Mytilus edulis*, Fig. 2). The spectrum produced by foraminiferal Mg is most similar to that produced by dolomitic Mg (Fig. 5). Dolomite ($(CaMg)(CO_3)_2$) has the same mineral structure as calcite, with Ca and Mg occupying equivalent octahedral sites in the lattice; Mg is ideally substituted for Ca. It is important to emphasise that the similarity to the dolomite spectrum indicates that the *local atomic environment*, or *coordination* of Mg is similar, not that dolomite is

present in the test structure. A survey of Mg spectra in the literature (Farges et al., 2009; Finch and Allison, 2008, 2007; Trcera et al., 2009) confirms that the only published NEXAFS Mg spectra that bears a resemblance to foraminiferal Mg are dolomite and Mg-calcite. One other notable candidate Mg coordination is that of northupite ($Na_3Mg(CO_3)_2Cl$, seen in Farges et al., 2009), which produces a similar spectrum to dolomite. However, this similarity is only superficial, as is evident from examination of the 'D' peak of the spectra (∼1330 eV in Farges' dolomite, ∼1322 eV in our dolomite, owing to differences in energy calibration). The D peak of northupite is at lower energy than the D peak of dolomite, and we observe a shift in the opposite direction in our foraminiferal calcite (Fig. 2, relative to dolomite). If the 'extra' on-band Mg were hosted in a northupite-like coordination, this would be manifest in a split D peak in the on-band spectra, which we do not see. The literature also reveals that NEXAFS is capable of detecting disordered organic-bound Mg in carbonate minerals (Farges et al., 2009; Finch and Allison, 2008). This reveals that Mg is ideally substituted for Ca in foraminiferal calcite, and validates the long-held assumption underpinning the Mg/Ca proxy.

The dolomite spectrum is not a perfect fit for foraminiferal Mg (Fig. 5). The goodness-of-fit (indicated by R^2 values in Fig. 5) is marginally improved in *A. lessonii* by including hydromagnesite ($Mg_5(CO_3)_4(OH)_2.4(H_2O)$) or magnesite ($MgCO_3$) Mg-environments alongside dolomite in the model (Fig. 5). The presence of a magnesite environment component would indicate Mg clustering, while a hydromagnesite environment suggests Mg associated with hydroxyl groups. Fitting a mixture of dolomite, magnesite and hydromagnesite spectra to the foraminiferal Mg, magnesite dominates the minor fit component in *A. lessonii*, while it is of similar importance as hydromagnesite in *O. universa* (although there is no improvement in goodness-of-fit in the latter, Fig. 5). This implies that Mg clustering may be more prominent in the higher-Mg calcite produced by *A. lessonii*. However, it is important to note that the shape of the fit residuals do not alter significantly with the addition of these extra environments, indicating that neither of these additional coordinations fully account for the differences between the Mg in dolomite and foraminiferal calcite. These disparities can be attributed to the compositional differences between dolomite (∼50% Mg) and foraminiferal calcite (<0.5% Mg), creating a different next-nearest-neighbour Mg environment in the crystal structure (Finch and Allison, 2007). The increase in goodness-of-fit in the two- and three-phase mixtures are so small that the interpretation of these minor phase components must remain tentative. We conclude from these results that Mg is ideally substituted for Ca in foraminifera, with the caveat that a small fraction may be present in close proximity to other Mg atoms in the calcite, or in association with hydroxyl groups.

These results give insights into the calcification processes of foraminifera. We conclusively demonstrate that banding is not caused by variations in the concentration of a separate, non-calcite Mg-bearing organic or mineral phase, or by the alternation between Mg being hosted in distinct coordinations (a two-phase Mg system). Intra-test Mg bands represent variations in the concentration of ideally substituted Mg in the calcite lattice. Therefore, they must either be the result of variations in the mechanism of crystal growth that affect Mg fractionation from the calcification fluid, or of changes in the chemical or physical mineralisation environment. The Mg/Ca palaeothermometer in its current form relies on the latter hypothesis, where changes in the physical environment (i.e. temperature) will effect the incorporation of Mg in a uniform way, despite biologically driven changes in solution chemistry. However, if the mechanism of crystal growth varies, so too will the sensitivity of Mg/Ca in different regions to temperature, and the ratio of on-band/off-band regions in the tests becomes a complicating factor that is not measured routinely in Mg/Ca analysis.

When combined with previous NEXAFS studies of Mg-calcites (Finch and Allison, 2007), our results provide strong evidence that the mechanism of crystal growth is constant in the foraminifera species studied here. An investigation of Mg in diverse inorganic calcite samples (Finch and Allison, 2007) revealed variations in Mg coordination that were detectable in NEXAFS spectra. These variations are not associated with differences in [Mg] between the inorganic calcites (Finch and Allison, 2007), indicating that they stem from differences in the mineral formation mechanism. Based on this observation, the degree of uniformity of Mg spectra gathered from on- and off-band regions in *A. lessonii* or *O. universa* (Fig. 4) implies the action of a single, continuous Mg incorporation (and therefore mineralisation) mechanism throughout the test structure. Furthermore, atomic force microscopy (AFM) studies of foraminiferal calcite (Cuif et al., 2012) report a uniform mosaic of ∼100 nm globular 'units' of calcite running throughout the test, in spite of compositional variations. If the mechanism of crystal growth varied significantly between compositional bands, we would expect to see some microstructural heterogeneity between on- and off-band regions, which is not observed. Together, these observations suggest that Mg is substituted into calcite by a uniform mechanism, and that Mg/Ca is entirely dependent on the physical and chemical calcification environment, rather than a variation in the mechanism of mineral growth.

This allows us to propose a working model of foraminiferal Mg incorporation, in which an ultimate connection between temperature and Mg/Ca is evident. In this model, the mineral in the whole test structure is deposited via a uniform crystallisation mechanism. Internal Mg heterogeneity is driven by variations in the chemistry of the calcification fluid, which stem from fluctuations in the biological mechanisms responsible for introducing the well-documented 'vital effect' Mg/Ca offsets (Weiner and Dove, 2003). For example, diurnal changes in the balance between organism respiration and symbiont photosynthesis can drive local pH changes of up to 1 unit, which would effect solution chemistry and crystal growth rate, and influence Mg incorporation (Eggins et al., 2004; Wolf-Gladrow et al., 1999). Inorganic precipitation experiments show that the incorporation of Mg into calcite is highly sensitive to the chemical mineralisation environment (Elhadj et al., 2006a; Katz, 1973; Mucci, 1987; Mucci and Morse, 1983; Stephenson et al., 2008), and that variations in calcification fluid chemistry would be sufficient to drive internal heterogeneity. The chemical environment can affect Mg incorporation in diverse ways, from simple increases in the concentration of Mg in the fluid (Mucci and Morse, 1983), to changes in the pH, saturation state and crystal growth rate (Burton and Walter, 1991), to considerably more complex interactions between defects on crystal growth faces and organic ligands (Elhadj et al., 2006b; Stephenson et al., 2008) or other trace cations (Stephenson et al., 2011). Our data cannot reveal which aspect of solution chemistry drives internal Mg/Ca variations, which are undoubtedly important in determining whole test Mg/Ca. Beyond these local variations in the chemical mineralisation environment, ocean temperature exerts a constant influence over the physical environment of crystal growth. Irrespective of the chemistry of the calcification fluid, and the mechanism by which Mg/Ca incorporation is modulated, temperature will affect the amount of Mg incorporated into the calcite lattice, following the basic thermodynamic and kinetic principles underlying an endothermic substitution. The fact that Mg is hosted in a calcite lattice means that temperature will always influence the amount of Mg incorporated into the calcite, relative to the solution the calcite is precipitating from. Furthermore, the enhanced temperature sensitivity of foraminiferal Mg/Ca (Lea et al., 1999) (cf. inorganic precipitation experiments) reveals that the biological mechanisms controlling the calcification fluid are also temperature sensitive (Bentov and Erez, 2006), and act to amplify foraminiferal Mg/Ca. Id est, if the

water is warmer, foraminiferal Mg/Ca will increase in both on-band and off-band regions (or vice versa), as a result of temperature driven changes in the kinetics of crystal growth, and the chemistry of the calcification fluid. Thus, ocean temperature influences the Mg/Ca of the whole test, in spite of local Mg/Ca variations.

5. Conclusions

Our results provide a fundamental step towards a mechanistic understanding of the Mg/Ca paleotemperature proxy and biomineralisation. By conclusively demonstrating the ideal substitution of Mg into the calcite lattice we have confirmed a long-held, yet untested assumption behind the Mg/Ca proxy, supporting the presence of an inorganic thermodynamic connection between seawater temperature and foraminiferal Mg/Ca. We demonstrate that foraminiferal Mg is not hosted in organic molecules, or in a secondary interstitial mineral or organic environment. Furthermore, the consistency of the Mg coordination throughout the test indicates that foraminifera employ a uniform mechanism of crystal growth. This supports the links between calcite-bound trace elements (like Mg) and the external environment upon which palaeoproxies rely.

Acknowledgements

Appendix A. Supplementary material

Supplementary material related to this article can be found online at http://dx.doi.org/10.1016/j.epsl.2013.09.037.

References

Anand, P., Elderfield, H., Conte, M., 2003. Calibration of Mg/Ca thermometry in planktonic foraminifera from a sediment trap time series. Paleoceanography 18, 28–31.

Bentov, S., Erez, J., 2006. Impact of biomineralization processes on the Mg content of foraminiferal shells: A biological perspective. Geochem. Geophys. Geosyst. 7, Q01P08.

Benzerara, K., Menguy, N., Obst, M., Stolarski, J., Mazur, M., Tyliszczak, T., Brown Jr., G.E., Meibom, A., 2011. Study of the crystallographic architecture of corals at the nanoscale by scanning transmission X-ray microscopy and transmission electron microscopy. Ultramicroscopy 111, 1268–1275.

Bluhm, H., Andersson, K., Araki, T., Benzerara, K., Brown, G., Dynes, J., Ghosal, S., Gilles, M., Hansen, H., Hemminger, J., Hitchcock, A., Ketteler, G., Kilcoyne, A., Kneedler, E., Lawrence, J., Leppard, G., Majzlan, J., Mun, B., Myneni, S., Nilsson, A., Ogasawara, H., Ogletree, D., Pecher, K., Salmeron, M., Shuh, D., Tonner, B., Tyliszczak, T., Warwick, T., Yoon, T., 2006. Soft X-ray microscopy and spectroscopy at the molecular environmental science beamline at the Advanced Light Source. J. Electron Spectrosc. Relat. Phenom. 150, 86–104.

Bohaty, S.M., Zachos, J.C., Delaney, M.L., 2012. Foraminiferal Mg/Ca evidence for Southern Ocean cooling across the Eocene–Oligocene transition. Earth Planet. Sci. Lett. 317–318, 251–261.

Burton, E.A., Walter, L.M., 1991. The effects of pCO_2 and temperature on magnesium incorporation in calcite in seawater and $MgCl_2$–$CaCl_2$ solutions. Geochim. Cosmochim. Acta 55, 777–785.

Cuif, J.-P., Dauphin, Y., Nehrke, G., Nouet, J., Perez-Huerta, A., 2012. Layered growth and crystallization in calcareous biominerals: impact of structural and chemical evidence on two major concepts in invertebrate biomineralization studies. Minerals 2, 11–39.

Eggins, S., Sadekov, A., de Deckker, P., 2004. Modulation and daily banding of Mg/Ca in Orbulina universa tests by symbiont photosynthesis and respiration: a complication for seawater thermometery?. Earth Planet. Sci. Lett. 225, 411–419.

Elderfield, H., Ganssen, G., 2000. Past temperature and $\delta^{18}O$ of surface ocean waters inferred from foraminiferal Mg/Ca ratios. Nature 405, 442–445.

Elderfield, H., Vautravers, M., Cooper, M., 2002. The relationship between shell size and Mg/Ca, Sr/Ca, $\delta^{18}O$, and $\delta^{13}C$ of species of planktonic foraminifera. Geochem. Geophys. Geosyst. 3, 1052.

Elderfield, H., Yu, J., Anand, P., Kiefer, T., Nyland, B., 2006. Calibrations for benthic foraminiferal Mg/Ca paleothermometry and the carbonate ion hypothesis. Earth Planet. Sci. Lett. 250, 633–649.

Elhadj, S., De Yoreo, J.J., Hoyer, J.R., Dove, P.M., 2006a. Role of molecular charge and hydrophilicity in regulating the kinetics of crystal growth. Proc. Natl. Acad. Sci. USA 103, 19237–19242.

Elhadj, S., Salter, E.A., Wierzbicki, A., De Yoreo, J.J., Han, N., Dove, P.M., 2006b. Peptide controls on calcite mineralization: polyaspartate chain length affects growth kinetics and acts as a stereochemical switch on morphology. Cryst. Growth Des. 6, 197–201.

Erez, J., 2003. The source of ions for biomineralization in foraminifera and their implications for paleoceanographic proxies. Rev. Mineral. Geochem. 54, 115–149.

Farges, F., Meibom, A., Flank, A., Lagarde, P., Janousch, M., Stolarski, J., 2009. Speciation of Mg in biogenic calcium carbonates. J. Phys. Conf. Ser. 190, 012175.

Finch, A.A., Allison, N., 2007. Coordination of Sr and Mg in calcite and aragonite. Mineral. Mag. 71, 539–552.

Finch, A.A., Allison, N., 2008. Mg structural state in coral aragonite and implications for the paleoenvironmental proxy. Geophys. Res. Lett. 35, L08704.

Gao, Q., Zhang, M., Niou, C., Li, M., Chien, K., 2004. Sidewall damage induced by FIB milling during TEM sample preparation. Presented at the Annual Proceedings – Reliability Physics (Symposium), pp. 613–614.

Garidel-thoron, T.D., Rosenthal, Y., Bassinot, F., Beaufort, L., 2005. Stable sea surface temperatures in the western Pacific warm pool over the past 1.75 million years. Nature 433, 294–298.

Giannuzzi, L.A., Geurts, R., Ringnalda, J., 2005. 2 keV Ga$^+$ FIB milling for reducing amorphous damage in silicon. Microsc. Microanal. 11.

Hintz, C.J., Shaw, T.J., Chandler, G.T., Bernhard, J.M., Mccorkle, D.C., Blanks, J.K., 2006. Trace/minor element: calcium ratios in cultured benthic foraminifera. Part I: Inter-species and inter-individual variability. Geochim. Cosmochim. Acta 70, 1952–1963.

Hitchcock, A.P., 1997. aXis2000 is free for non-commercial use. It is written in Interactive Data Language (IDL) and available from http://unicorn.mcmaster.ca/aXis2000.html.

Hitchcock, A., Tyliszczak, T., Obst, M., Swerhone, G., Lawrence, J., 2010. Improving sensitivity in soft X-ray STXM using low energy X-ray fluorescence. Microsc. Microanal. 16, 924–925.

Katz, A., 1973. The interaction of magnesium with calcite during crystal growth at 25–90 °C and one atmosphere. Geochim. Cosmochim. Acta 37, 1563–1586.

Kısakürek, B., Eisenhauer, A., Böhm, F., Garbe-Schönberg, D., Erez, J., 2008. Controls on shell Mg/Ca and Sr/Ca in cultured planktonic foraminiferan, Globigerinoides ruber (white). Earth Planet. Sci. Lett. 273, 260–269.

Kudo, M., Kameda, J., Saruwatari, K., Ozaki, N., Okano, K., Nagasawa, H., Kogure, T., 2010. Microtexture of larval shell of oyster, Crassostrea nippona: A FIB-TEM study. J. Struct. Biol. 169, 1–5.

Kunioka, D., Shirai, K., Takahata, N., Sano, Y., Toyofuku, T., Ujiie, Y., 2006. Microdistribution of Mg/Ca, Sr/Ca, and Ba/Ca ratios in Pulleniatina obliquiloculata test by using a NanoSIMS: Implication for the vital effect mechanism. Geochem. Geophys. Geosyst. 7, Q12P20.

Lea, D.W., Mashiotta, T., Spero, H., 1999. Controls on magnesium and strontium uptake in planktonic foraminifera determined by live culturing. Geochim. Cosmochim. Acta 63, 2369–2379.

Lea, D.W., Pak, D.K., Spero, H.J., 2000. Climate impact of late quaternary equatorial Pacific Sea surface temperature variations. Science 289, 1719–1724.

McCaffrey, J.P., Phaneuf, M.W., Madsen, L.D., 2001. Surface damage formation during ion-beam thinning of samples for transmission electron microscopy. Ultramicroscopy 87, 97–104.

Morse, J., Bender, M., 1990. Partition-coefficients in calcite: examination of factors influencing the validity of experimental results and their application to natural systems. Chem. Geol. 82, 265–277.

Mucci, A., 1987. Influence of temperature on the composition of magnesian calcite overgrowths precipitated from seawater. Geochim. Cosmochim. Acta 51, 1977–1984.

Mucci, A., Morse, W., 1983. The incorporation of Mg^{2+} and Sr^{2+} into calcite overgrowths: influences of growth rate and solution composition. Geochim. Cosmochim. Acta 47, 217–233.

Nürnberg, D., Bijma, J., Hemleben, C., 1996. Assessing the reliability of magnesium in foraminiferal calcite as a proxy for water mass temperatures. Geochim. Cosmochim. Acta 60, 803–814.

Nürnberg, D., Müller, A., Schneider, R., 2000. Paleo-sea surface temperature calculations in the equatorial east Atlantic from Mg/Ca ratios in planktic foraminifera:

A comparison to sea surface temperature estimates from Uk37, oxygen isotopes, and foraminiferal transfer function. Paleoceanography 15, 124–134.

Obst, M., Dynes, J.J., Lawrence, J.R., Swerhone, G.D.W., Benzerara, K., Karunakaran , C., Kaznatcheev, K., Tyliszczak, T., Hitchcock, A.P., 2009. Precipitation of amorphous $CaCO_3$ (aragonite-like) by cyanobacteria: A STXM study of the influence of EPS on the nucleation process. Geochim. Cosmochim. Acta 73, 4180–4198.

R Core Team, 2012. R: A Language and Environment for Statistical Computing. R Foundation for Statistical Computing, Vienna, Austria.

Reyntjens, S., 2006. TEM Preparation Notes. FEI.

RStudio, 2013. RStudio: Integrated development environment for R. Version 0.96.330.

Russell, A.D., Hönisch, B., Spero, H.J., Lea, D.W., 2004. Effects of seawater carbonate ion concentration and temperature on shell U, Mg, and Sr in cultured planktonic foraminifera. Geochim. Cosmochim. Acta 68, 4347–4361.

Sadekov, A.Y., Eggins, S.M., de Deckker, P., 2005. Characterization of Mg/Ca distributions in planktonic foraminifera species by electron microprobe mapping. Geochem. Geophys. Geosyst. 6, Q12P06.

Stephenson, A.E., DeYoreo, J.J., Wu, L., Wu, K.J., Hoyer, J., Dove, P.M., 2008. Peptides enhance magnesium signature in calcite: insights into origins of vital effects. Science 322, 724–727.

Stephenson, A.E., Hunter, J.L., Han, N., DeYoreo, J.J., Dove, P.M., 2011. Effect of ionic strength on the Mg content of calcite: Toward a physical basis for minor element uptake during step growth. Geochim. Cosmochim. Acta 75, 4340–4350.

Trcera, N., Cabaret, D., Rossano, S., Farges, F., Flank, A.-M., Lagarde, P., 2009. Experimental and theoretical study of the structural environment of magnesium in minerals and silicate glasses using X-ray absorption near-edge structure. Phys. Chem. Miner. 36, 241–257.

Urey, H.C., Lowenstam, H.A., Epstein, S., McKinney, C.R., 1951. Measurement of paleotemperatures and temperatures of the upper cretaceous of England, Denmark, and the southeastern United States. Geol. Soc. Am. Bull. 62, 399–416.

Weiner, S., Dove, P., 2003. An overview of biomineralization processes and the problem of the vital effect. Rev. Mineral. Geochem. 54, 1.

Wolf-Gladrow, D., Bijma, J., Zeebe, R., 1999. Model simulation of the carbonate chemistry in the microenvironment of symbiont bearing foraminifera. Mar. Chem. 64, 181–198.